Fast synthesis of TiNi by mechanical alloying and its hydrogenation properties

Tohru Nobuki, Jean-Claude Crivello, Fermin Cuevas, Jean-Marc Joubert

Available online at www.sciencedirect.com

ScienceDirect

journal homepage: www.elsevier.com/locate/he

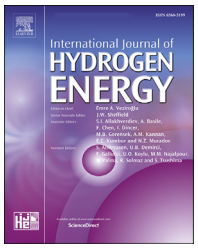

Fast synthesis of TiNi by mechanical alloying and its hydrogenation properties

Tohru Nobuki [a,b,*], *Jean-Claude Crivello* [a], *Fermin Cuevas* [a], *Jean-Marc Joubert* [a]

[a] *Université Paris Est, ICMPE (UMR 7182), CNRS, UPEC, F-94320 Thiais, France*
[b] *Faculty of Engineering, Kindai University, 1 Takaya-Umenobe, Higashi-Hiroshima City, 739-2116, Japan*

ARTICLE INFO

Article history:
Received 7 January 2019
Received in revised form
22 February 2019
Accepted 25 February 2019
Available online 20 March 2019

Keywords:
Mechanical alloying
TiNi
Hydrogen storage

ABSTRACT

Mechanical alloying is widely used for the synthesis of hydrogen storage materials. However, amorphization and contamination triggered by long-time milling are serious drawbacks for obtaining efficient hydrogen storage. In this work, short-time ball milling synthesis is explored for a representative hydride forming compound: TiNi. Through structural, morphological and chemical characterizations, we evidence that formation of TiNi is complete in only 20 min with minor Fe contamination (0.2 wt%). Cross-sectional analysis of powder stuck on milling balls reveals that alloy formation occurs through the interdiffusion between thin layers of co-laminated pure elements. Hydrogenation thermodynamics and kinetics of short-time mechanically alloyed TiNi are similar to those of coarse-grained compounds obtained by classical high-temperature melting. Mechanical alloying is a suitable method for fast and energy-efficient synthesis of intermetallic compounds such as TiNi.

Introduction

Mechanical alloying (MA) is a popular method to produce hydride-forming AB_n compounds such as $LaNi_5$, ZrV_2 TiFe, and Mg_2Ni with $n = 5$, 2, 1 and 0.5, respectively. MA is a solid-state powder processing technique, which involves repeated welding, fracturing and re-welding of powder particles in a high-energy ball mill [1,2]. The so-obtained hydride-forming compounds have fast absorption and desorption kinetics, even at relatively low temperatures [3]. However, their reversible hydrogen storage capacity is often reduced due to alloy amorphization [4–6].

Among the different types of *AB* hydride-forming compounds, TiNi-type alloys are the most promising electrode materials for Nickel-Metal Hydride (Ni-MH) batteries [7–10]. TiNi-type alloys have also been extensively investigated due to its shape memory characteristics [11,12] and hydrogen storage performance [13–15]. As concerns hydrogen storage, it is known that both TiNi and Ti_2Ni intermetallics in the Ti–Ni system absorb hydrogen at room temperature [16]. TiNi alloy has a reversible hydrogenation capacity of 0.7 hydrogen per metal atom (H/M). Ti_2Ni alloy absorbs up to 0.83 H/M but formed hydrides have high thermodynamic stability and poor kinetics [17,18]. It was reported that amorphization and contamination during a long MA process may reduce the

* *Corresponding author.*
E-mail address: nobuki@hiro.kindai.ac.jp (T. Nobuki).
https://doi.org/10.1016/j.ijhydene.2019.02.203

hydrogen capacity and kinetics [19]. Consequently, reports on hydrogenation properties of TiNi alloy synthesized by MA are scarce [20,21].

This work aims to study the alloying process of TiNi by high energy ball milling. Besides clarifying the alloy formation mechanism, the target is to reduce the milling time in order to avoid amorphization and minimize contamination from the milling tools. The hydrogenation properties of short-time mechanically alloyed TiNi are determined and compared to those of coarse-grained TiNi reported in the literature.

Experimental procedure

High purity elemental powders of titanium (99.5%, <37 μm, CERAC) and nickel (99.9%, <44 μm, NEYCO) were used. The Ti and Ni powder mixture (3.0 g) in stoichiometric amount was mechanically milled to obtain TiNi intermetallic compound using 86 stainless steel balls (diameter: 7 mm, ball-to-powder ratio: 40:1) in a hardened stainless-steel vial. The vial was sealed in a glove box under argon atmosphere. The high-energy planetary ball milling equipment (Premium line P7, Fritsch) was run at 800 rpm for different periods of time following the timeline displayed in Fig. 1. At each milling-time step, the powder was scraped from the balls and the vial wall. The agglomerated material was crushed, and intermediate picking of the sample was carried out for analysis. Milling balls were also taken after 6, 12 and 56 min, cut in the equatorial plane, embedded in resin and polished for subsequent analysis. Inspired by other works [22–24], 1-h stop between milling steps was defined to reduce sample heating and to dissipate the heat.

An Optical Microscope (OM, ZEISS Axio Observer Z1m) and a Field Emission Scanning Electron Microscope (FE-SEM/EDX MERLIN Gemini 2, ZEISS) was used to analyze the morphology and chemical composition of the MA powder stuck to the milling balls. For morphological studies, Back-Scattering Electron (BSE) images of the milling ball cross sections were monitored. Elemental chemical analysis was obtained Energy-Dispersed X-rays (EDX). Average Fe contamination of milled powders was determined by Inductively Coupled Plasma Optical Emission Spectroscopy (ICP-OES, Varian VistaPro). The phase identification of the powder samples was carried out using X-ray diffraction (XRD) analysis with a Bragg–Brentano θ-θ diffractometer (D8 Advance Bruker) using Cu-Kα radiation operated at 40 mA and 40 kV. Phase identification and refinement of lattice parameters were carried out by the Rietveld Method using FullProf software [25].

Hydrogenation properties of the synthesized alloy were measured using a homemade manometric Sieverts-type apparatus. The sample weight was about 0.3 g. The measurements were performed at 100, 150 and 200 °C for hydrogen pressure comprised between 0.01 and 100 bar.

Results and discussion

TiNi synthesis by mechanical alloying

The XRD results at different milling time are presented in Fig. 2. From the peaks indexation, the B2–TiNi phase appears after 12 min of milling. After 20 min, the TiNi formation is complete since neither diffraction peaks of *fcc* Ni nor *hcp* Ti are detected. For longer milling time, the only modification observed is the peak-broadening attributed to both crystallite size reduction and the increase of strains.

The sample after 30 min of milling has been measured by XRD with a longer acquisition time to improve diffraction statistics and perform Rietveld analysis as displayed in Fig. 3. The refined lattice parameter $a = 0.3014$ nm agrees with literature data [26]. Such a Rietveld analysis was also carried out on the other milled samples (not shown). Phase amounts were obtained from this analysis and are shown in Fig. 4. The

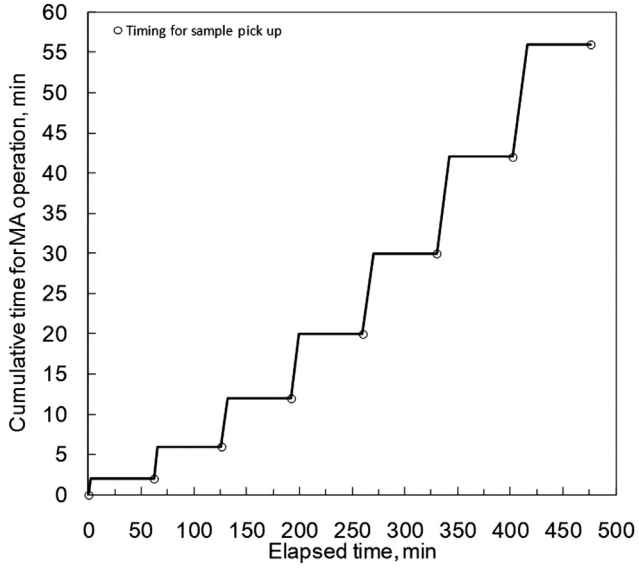

Fig. 1 – Timeline showing the different steps of the MA synthesis. A sample was removed at each step to carry out analysis.

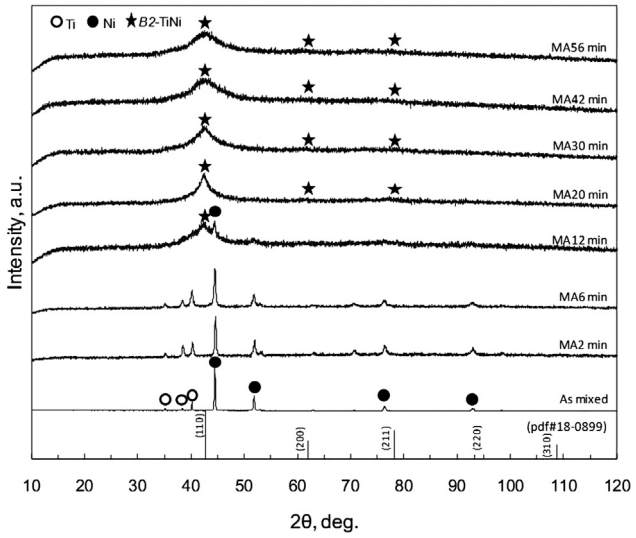

Fig. 2 – XRD diffraction patterns at different milling time during TiNi synthesis by MA.

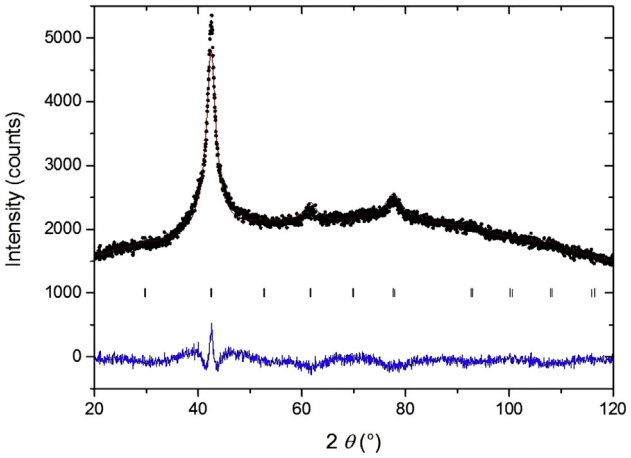

Fig. 3 – Graphical output of the Rietveld analysis after 30min of MA. Observed (points), calculated (line) and difference (line below) curves are shown. The vertical bars indicate the peak position of TiNi phase with *B2* type structure.

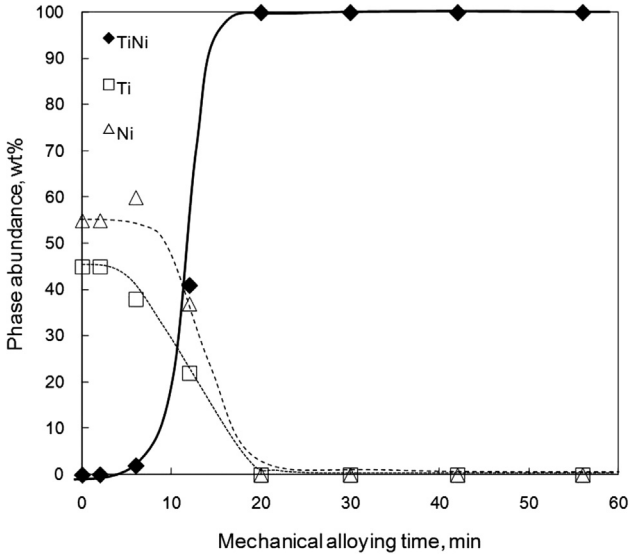

Fig. 4 – Phase abundance from Rietveld analysis of Ti–Ni powders as a function of milling time.

mechanochemically-induced reaction Ti + Ni → TiNi takes place between 6 and 20 min of milling time.

Optical microscope images of the interface between a milling ball and Ti–Ni powder at different milling time are displayed in Fig. 5. After 6 min, a layered structure stuck on the entire ball surface was observed. The thickness is around 100 μm, *i.e.* much larger than initial powder size of Ti or Ni. After 12 min, the structure is less homogeneous reaching 200 μm thickness in some places while in other places no material is stuck on the ball. Finally, after 56 min, only very few and very thin (20 μm) islands of material are still attached to the ball.

The same samples were examined by SEM using BSE images and EDX elemental mapping as well as EDX point analysis (Fig. 6). After 6 min, the sample has a multilayered structure. The observed contrast is attributed to the difference in the electronic density between Ti (darker) and Ni (brighter). Very thin in some places, wider in some other places, Ti and Ni layers are always observed confirming that, at this step, no intermetallic compound has been formed. The analysis points no3 and 4, giving close to equi-atomic TiNi composition are an average between the different layers of pure Ti and Ni whose thickness is much lower than the resolution of the measurement (typically 1 μm). After 12 min, Ti and Ni layers are still observed on both the interface between the ball and the stuck powder as well as on the outer surface. Between this, a homogenous region is seen whose composition matches the expected TiNi equiatomic composition (45 wt% Ti, 55 wt% Ni) indicating the formation of the intermetallic compound. After 56 min, homogeneous TiNi composition is observed at some locations. Fe contamination is also detected by EDX. To determine the global Fe contamination in the milled powders, ICP-OES chemical analysis was done. Fe content as a function of milling time is displayed in Fig. 7. Fe content gradually increases from 0.01 to 0.29 wt% for milling time ranging from 0 to 56 min. When TiNi formation is complete, *i.e.* after 20 min of milling, Fe-content is rather low: 0.20 ± 0.01 wt%.

The previous SEM results are not only in perfect agreement with the phase identification and quantification obtained by XRD (Figs. 2–4) but also elucidate the mechanism of TiNi synthesis by mechanical alloying. TiNi synthesis proceeds by the formation and interdiffusion between thinner and thinner layers of co-laminated pure elements. In the initial period, flaked Ni and Ti elements are fixed to the surface of the balls. Then, between 6 and 12 min, the elongated flaked elements were layered and grew up by cold welding through ball collisions yielding thinner and thinner layers. Below a given thickness limit, the two-phase lamellar structure collapse into a single TiNi phase for milling time longer than 20 min. Analogous solid-state reaction mechanism on decreasing the Ti/Ni layer thickness has been observed in Ti–Ni multilayered thin film structures [27]. This mechanism is a typical behavior of alloy formation by mechanical milling in ductile-ductile systems such as Ag-Cu [2] and Al-Fe [28]. The occurrence of an intimate two-phase lamellar structure as precursor of TiNi formation concurs with previous studies of Zhao et al. by mechanical alloying [29]. However, the milling conditions used in our experiment are much more energetic than those used by Zhao et al. leading to dissimilar outcomes on TiNi formation. Indeed, we used much higher vial rotation speed (800 rpm) and ball-to-powder ratio (40:1) as compared to those employed by Zhao et al. (250 rpm and 20:1, respectively). TiNi formation here reported takes only in 20 min whereas 100 h were needed by Zhao et al.. Moreover, by using our high-energy milling conditions, TiNi is obtained in crystalline form whereas it forms an amorphous phase at low-energy milling [29]. Such a difference is evidenced by the fact that three distinct diffraction peaks belonging to *B2* structure are here observed within the angular range $20 \leq 2\theta \leq 80°$ (Fig. 4), whereas a unique and very broad diffraction bump at ~45° was observed by Zhao et al.. This discrepancy may tentatively be assigned to higher local temperature at impact between metal powders and balls with increasing milling energy, which might lead to recrystallization processes.

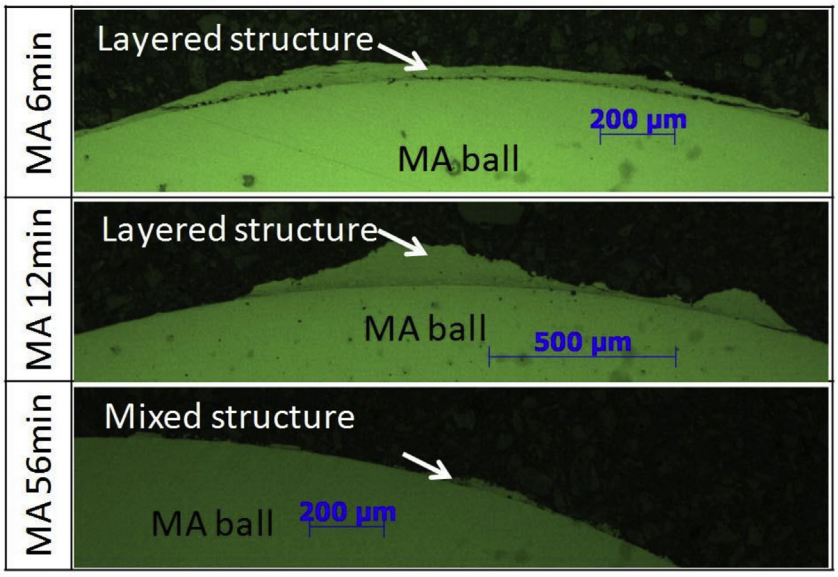

Fig. 5 – Cross-section optical microscope images of the interface between stainless-steel ball and MA Ti–Ni powder at different milling time.

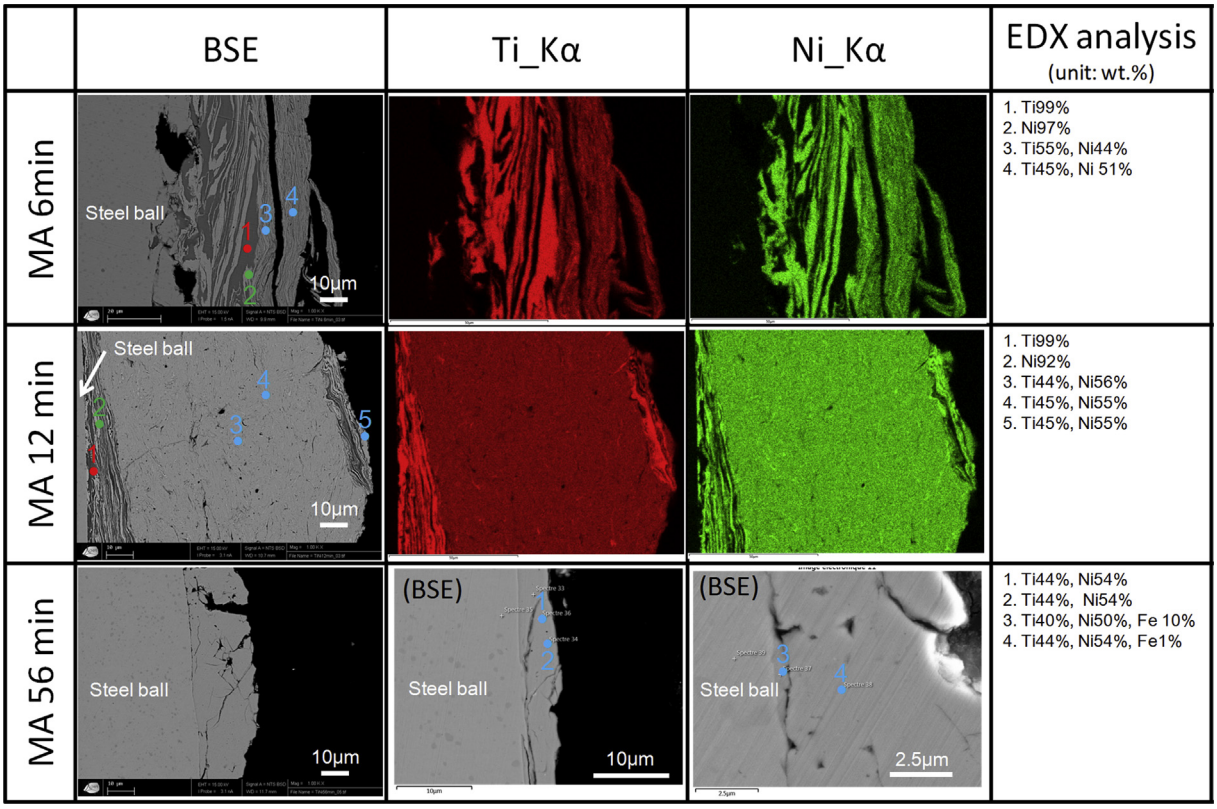

Fig. 6 – Cross-section SEMEDX analysis of the interface between stainless-steel ball and MA Ti–Ni powder at different milling time.

Hydrogenation properties of MA TiNi

The previous structural, morphological and analytical characterization of mechanically alloyed Ti–Ni powders demonstrates that complete and chemically homogeneous TiNi formation is achieved at 30 min of milling. As a next step, the hydrogenation properties of this sample were measured with a Sieverts apparatus. The sample was first activated by doing three hydrogenation cycles. Each cycle consists of hydrogen absorption (P_{H2} = 80 bar for 1 h at 300 °C and cooling down to room temperature RT) and desorption (primary vacuum at 300 °C for 0.5 h) sweeps. Then, Pressure-Composition-

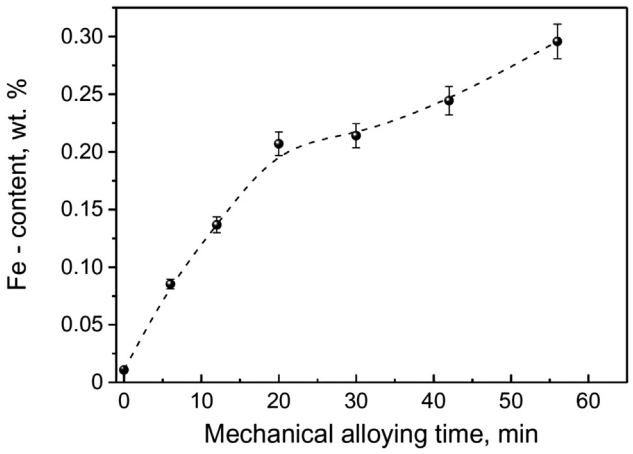

Fig. 7 – Iron content as a function of milling time determined by ICP-OES. Dashed line is a guide for the eye.

Temperature (PCT) isotherms were measured at 100 °C, 150 °C and 200 °C and are displayed in Fig. 8. No pressure plateau is observed. The capacity is significantly higher at low temperature where a considerable hysteresis is noticed and attributed to the failure to reach equilibrium during the desorption due to the slow kinetics. At high temperature (T ≥ 150 °C) hysteresis effects diminish and a good reversibility is observed upon hydrogen absorption and desorption. The comparison with literature reference data [13] obtained for a cast and annealed alloy show that quite similar properties in terms of capacity and stability are obtained with our alloy synthesized by MA. This suggests that the reduced crystallinity of MA sample does not modify significantly the thermodynamics of the H–TiNi system. The hydrogenation kinetics were then measured upon hydrogen absorption at 100 bar after dehydrogenation treatment (200 °C, overnight, primary vacuum). They are shown in Fig. 9 at 100 °C and 200 °C. At 200 °C, the reaction is pretty fast but is significantly slower at 100 °C. Indeed, hydrogenation kinetics of TiNi are reported to be as fast as those of TiFe at high temperatures [30]

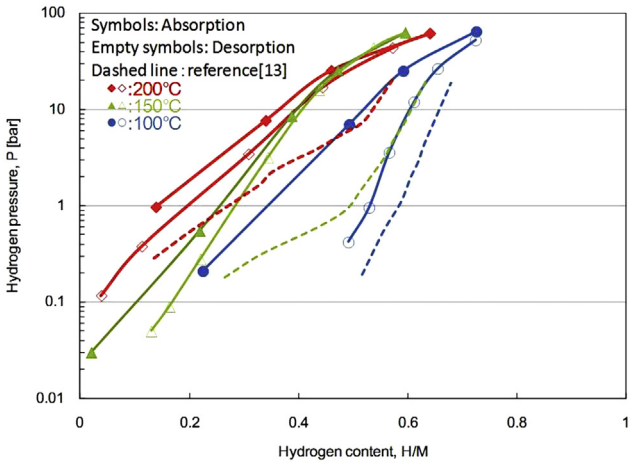

Fig. 8 – Pressure-Composition-Temperature isotherms both on absorption (solid symbols) and desorption (empty symbols) and their comparison with literature data of Coarse-grained TiNi on desorption [13].

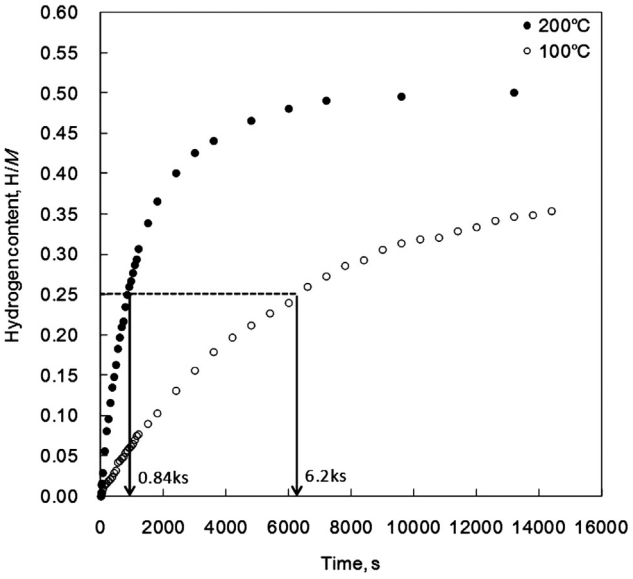

Fig. 9 – Hydrogen absorption under 100 bar as a function of time at 100 °C and 200 °C. The half-time for complete absorption is indicated.

(T ≥ 500 °C) but it slows down when approaching RT conditions [14,31].

After all previous hydrogenation measurements, the sample was fully charged with hydrogen at 100 °C and 100 bar of hydrogen pressure for 72 h. It was then cooled down to RT, evacuated and extracted from the sample holder to be characterized by XRD. Fig. 10 shows the Rietveld analysis of this sample. The diffraction pattern is perfectly indexed using the structure of TiNiH as published by Soubeyroux et al. with space group *I4/mmm* [14]. The refined lattice parameters ($a = 0.6234$ nm, $c = 1.2416$ nm) are higher than those reported for TiNiH ($a = 0.6217$ nm, $c = 1.2326$ nm). Indeed, they are much closer to those reported for the same authors for deuteride $TiNiD_{1.4}$ ($a = 0.6236$ nm, $c = 1.2424$ nm) suggesting full

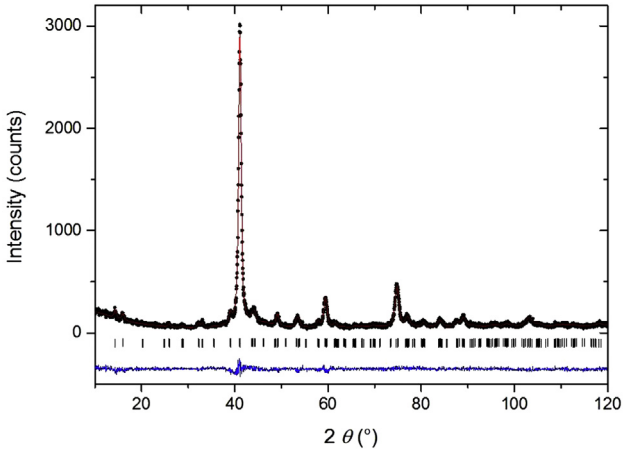

Fig. 10 – Rietveld refinement of fully hydrogenated TiNi alloy synthesized by short-time (30 min) MA. Observed (points), calculated (line) and difference (line below) curves are shown. The vertical bars indicate the peak positions of TiNiH phase [ref 14].

saturation in hydrogen at the imposed thermodynamic conditions. It is important to note the much better crystalline quality of the hydride (sharper diffraction peaks) compared to the as-milled material (see Fig. 3) showing the influence of hydrogen on the reduction of inhomogeneities and strains of the initial material. This concurs with recent studies on hydrogen-induced accelerated grain growth in metals [32], though thermal annealing effects during the measurement of hydrogenation properties cannot be ruled out.

Conclusions

We successfully synthesized TiNi compound by mechanical alloying of the metallic elements and measured its hydrogenation properties. A milling time of 20 min was enough to obtain single-phase TiNi while minimizing Fe contamination. The mechanical alloying mechanism, *i.e.* solid-state reaction between thin Ti and Ni multilayered structure, could be evidenced through an original approach which consists in characterizing the microstructure and composition of the milled materials attached to the balls as a function of milling time. Hydrogenation thermodynamic properties and kinetics were comparable to literature data for coarse-grained alloys prepared by classical melting techniques. Mechanical alloying can be therefore considered as a fast and energy efficient synthetic route for the synthesis of TiNi powders of high purity with remarkable hydrogenation properties.

Acknowledgements

Rémi Pires and Junxian Zhang are gratefully acknowledged for SEM/EDX and ICP analysis, respectively.

REFERENCES

[1] Benjamin JS. Mechanical alloying. Sci Am 1976;234:40–9. https://doi:10.1038/scientificamerican0576-40.
[2] Suryanarayana C. Mechanical alloying and milling. Prog Mater Sci 2001;46:1–184. https://DOI:10.1016/S0079-6425(99)00010-9.
[3] Huot J, Ravnsbæk DB, Zhang J, Cuevas F, Latroche M, Jensen TR. Mechanochemical synthesis of hydrogen storage materials. Prog Mater Sci 2013;58:30–75. https://DOI:10.1016/j.pmatsci.2012.07.001.
[4] Zaluski L, Zaluska A, Ström-Olsen JO. Nanocrystalline metal hydrides. J Alloy Compd 1997;253–254:70–9. https://doi.org/10.1016/S0925-8388(96)02985-4.
[5] Fujii H, Munehiro S, Fujii K, Orimo S. Effect of mechanical grinding under Ar and H_2 atmospheres on structural and hydriding properties in $LaNi_5$. J Alloy Compd 2002;330–332:747–51. https://doi.org/10.1016/S0925-8388(01)01508-0.
[6] Liang G, Huot J, Schulz R. Hydrogen storage properties of the mechanically alloyed $LaNi_5$-based materials. J Alloy Compd 2001;230:133–9. https://doi.org/10.1016/S0925-8388(01)00929-X.
[7] Makowiecka M, Jankowska E, Okonska I, Jurczyk M. Effect of Zr additions on the electrode characteristics of nanocrystalline TiNi-type hydrogen storage alloys. J Alloy Compd 2005;388:303–7. https://doi.org/10.1016/j.jallcom.2004.07.026.
[8] Guiose B, Cuevas F, Décamps B, Leroy E, Percheron-Guégan A. Microstructural analysis of the ageing of pseudo-binary (Ti,Zr)Ni intermetallic compounds as negative electrodes of Ni-MH batteries. Electrochim Acta 2009;54:2781–9. https://doi.org/10.1016/j.electacta.2008.11.024.
[9] Emami H, Cuevas F, Latroche M. Ti(Ni,Cu) pseudobinary compounds as efficient negative electrodes for Ni-MH batteries. J Power Sources 2014;265:182–91. https://doi.org/10.1016/j.jpowsour.2014.04.114.
[10] Emami H, Cuevas F. Cobalt induced multi-plateau behavior in TiNi-based Ni-MH electrodes. Energy Storage Mater 2017;8:189–93. https://doi.org/10.1016/j.ensm.2016.11.008.
[11] Otsuka K, Ren X. Recent developments in the research of shape memory alloys. Intermetallics 1999;7:511–28. https://doi.org/10.1016/S0966-9795(98)00070-3.
[12] Van Humbeeck J. Shape memory alloys: a material and a technology. Adv Eng Mater 2001;3:837–50. <837::AID-ADEM837>3.0.CO;2-0, https://doi.org/10.1002/1527-2648(200111)3:11.
[13] Burch R, Mason NB. Absorption of hydrogen by titanium-cobalt and titanium-nickel intermetallic alloys. J Chem Soc Faraday Trans I 1979;75:561–77. http://doi.org/10.1039/F19797500561.
[14] Soubeyroux J-L, Fruchart D, Lorthioir G, Ochin P, Colin D. Structural study of the hydrides $NiTiH_x$ ($x = 1.0$ and 1.4). J Alloy Compd 1993;196:127–32. https://doi.org/10.1016/0925-8388(93)90582-8.
[15] Guiose B, Cuevas F, Décamps B, Percheron-Guégan A. Solid-gas and electrochemical hydrogenation properties of pseudo-binary (Ti,Zr)Ni intermetallic compounds. Int J Hydrogen Energy 2008;33:5795–800. https://doi.org/10.1016/j.ijhydene.2008.07.056.
[16] Luan B, Cui N, Zhao H, Zhong S, Liu HK, X Dou S. Studies on the performance of $Ti_2Ni_{1-x}Al_x$ hydrogen storage alloy electrodes. J Alloy Compd 1996;233:225–30. https://doi.org/10.1016/0925-8388(95)02054-3.
[17] Buchner H, Gutjahr MA, Beccu K-D, Säufferer H. Hydrogen in intermetallic phases: the system titanium-nickel-hydrogen. Z Metallkunde 1972;63:497–500.
[18] Gutjahr MA, Buchner H, Beccu KD, Säufferer H. A new type of reversible negative electrode for alkaline storage batteries based on metal alloy hydrides. Power Sources 1973;4:79–91.
[19] Zhao Xiangyu, Ma Liqun, Yang Meng, Ding Yi, Shen Xiaodong. Electrochemical properties of Ti-Ni-H powders prepared by milling titanium hydride and nickel. Int J Hydrogen Energy 2010;35:3076–9. https://doi.org/10.1016/j.ijhydene.2009.07.017.
[20] Suryanarayana C, Al-Aqeel Nasser. Mechanically alloyed nanocomposites. Prog Mater Sci 2013;58:383–502. https://doi.org/10.1016/j.pmatsci.2012.10.001.
[21] Bououdina M, Oumellal Y, Dupont L, Aymard L, Al-Gharni H, Al-Hajry A, Maark TA, De Sarkar A, Ahuja R, Deshpande MD, Qian Z, Rahane AB. Lithium storage in amorphous TiNi hydride: electrode for rechargeable lithium-ion batteries. Mater Chem Phys 2013;141:348–54. https://doi.org/10.1016/j.matchemphys.2013.05.021.
[22] Balcerzak M, Jakubowicz J, Kachlicki T, Jurczyk M. Hydrogenation properties of nanostructured Ti_2Ni-based alloys and nanocomposites. J Power Sources 2015;280:435–45. https://doi.org/10.1016/j.jpowsour.2015.01.135.
[23] Drenchev Boris, Tony Spassov. Electrochemical hydriding of amorphous and nanocrystalline TiNi-based alloys. J Alloy Compd 2007:441197–201. https://doi.org/10.1016/j.jallcom.2006.09.071.

[24] Takacs L, McHenry JS. Temperature of the milling balls in shaker and planetary mills. J Mater Sci 2006;41:5246–9. https://doi.org/10.1007/s10853-006-0312-4.
[25] Rodríguez-Carvajal Juan. Recent advances in magnetic structure determination by neutron powder diffraction. Phys B Condens Matter 1993;192:55–69. https://doi/10.1016/0921-4526(93)90108-I.
[26] Murray J-L. The Ni-Ti (Nickel-Titanium) system in phase diagrams of binary titanium alloys. In: Murray J-L, editor. Metals Park. Ohio: ASM International; 1987. p. 197–211.
[27] Bruce M. Clemens. Solid-state reaction and structure in compositionally modulated zirconium-nickel and titanium-nickel films. Phys RevB 1986;33:1. https://doi.org/10.1103/PhysRevB.33.7615.
[28] Bin H, Kobayashi KF, Shingu PH. Mechanical alloying and consolidation of aluminium-iron system. J Jpn Inst Light Metals 1988;38:165–71. https://doi.org/10.2464/jilm.38.165.
[29] Zhao X, Ma L, Gou Y, Shen X. Structure, morphology and hydrogen desorption characteristics of amorphous and crystalline Ti-Ni alloys. Mater Sci Eng 2009;516:50–3. https://doi.org/10.1016/j.msea.2009.04.015.
[30] Schmidt R, Schlereth M, Wipf H, Assmus W, Müllner M. Hydrogen solubility and diffusion in the shape-memory alloy NiTi. J Phys Condens Matter 1989;1:2473. https://doi.org/10.1088/0953-8984/1/14/003.
[31] Zlatanova Zlatina, Spassov Tony, Eggeler Gunther, Spassova Maya. Synthesis and hydriding/dehydriding properties of Mg_2Ni-AB (AB = TiNi or TiFe) nanocomposites. Int J Hydrogen Energy 2011;36:7559–66. https://doi.org/10.1016/j.ijhydene.2011.03.092.
[32] Martin May L, Pundt Astrid, Kirchheim Reiner. Hydrogen-induced accelerated grain growth in vanadium. Acta Mater 2018;155:262–8. https://doi.org/10.1016/j.actamat.2018.06.011.